Optical phonon production by upconversion: Heterojunction-transmitted versus native phonons

Seungha Shin[*]

Department of Mechanical, Aerospace and Biomedical Engineering, University of Tennessee, Knoxville, Tennessee 37996, USA

Massoud Kaviany

Department of Mechanical Engineering, University of Michigan, Ann Arbor, Michigan 48109, USA

High-energy optical phonons are preferred in phonon-absorbing transitions, and regarding their production we analyze the phonon upconversion processes under nonequilibrium created by heterojunction transmission. For heterojunctions, steady phonon flux from a low-cutoff-frequency layer (e.g., Ge) is transmitted to a high cutoff layer (e.g., Si), creating a nonequilibrium population of low-energy phonons for upconversion. Using quantum spectral phonon transmission and first-principles calculations of the phonon interaction kinetics, we identify the high-conversion efficiency channels, i.e., modes and wave vectors. Junction-transmitted phonons, despite suffering from the interface reflection and from spreading interactions with equilibrium native phonons, have a high upconversion rate to Brillouin zone-boundary optical phonons, while nonequilibrium native phonons are efficiently upconverted over most of the zone. So, depending on the harvested optical phonon, one of these nonequilibrium phonons can be selected for an efficient upconversion rate.

PACS number(s): 63.20.kg, 74.25.Kc, 79.60.Jv

I. INTRODUCTION

Phonons emitted by transiting and transitioning of energy carriers in solids create a local nonequilibrium (NE) population which will consequently be equilibrated by phonon-electron (p-e) [1], phonon-spin (p-s) [2], and phonon-phonon (p-p) interactions [3]. The p-p processes dominate with increased temperature and include phonon up- and downconversion, where, in three-phonon upconversion, two phonons are annihilated, creating one phonon with a higher energy (E_p) (the reverse occurs in downconversion) [4]. Upconversion can be explored for a resonant optical phonon source, analogous to photon upconversion, in which sequential absorption of two or more photons leads to emission of one with a higher energy [5]. Photon upconversion is used in infrared (IR)-to-visible conversion (e.g., in lasers) and in optical storage, although the efficiency is rather low [6], where the quantized electromagnetic wave interacts with electric (or magnetic) entities, leading to metastable excited states [7].

The p-p interaction kinetics is determined by the anharmonicity in the force field and the phonon population distribution under the conservation of momentum and energy. Up- and downconversion rates are balanced under equilibrium. So, for a desirable interaction characteristic (e.g., enhanced phonon upconversion under its absorption in energy conversion), the population distribution needs a controlled deviation from equilibrium. We examine the heterojunction structure for providing a distinct NE phonon population near the interface. We note that in homogeneous bulk solids this deviation from equilibrium is only noticeable under extreme local heating (differently from heterojunction transmission).

In this article, based on the interaction kinetics of low-energy phonon upconversion, we introduce a heterojunction phonon upconverter (HPUC) for efficient supply of optical phonons which have a higher energy and lower entropy.

High-energy, optical phonons can be harvested in unassisted resonant electronic transitions (phonon-tuned heterobarrier [8]) and in phonon-assisted photon absorption processes in semiconductors and in isolated rare-earth ions [9,10]. Other applications of resonance (optical) phonon absorption can include IR photon emission as the reverse of IR two-phonon emission [11,12], i.e., using phonon upconversion in an enhanced IR optical source. In these applications, harvested optical phonons are absorbed and converted to electronic energy.

In the HPUC system, low-energy phonons cross the junction into a high-energy layer (creating overpopulation), upconvert there, and then become absorbed (with steady underpopulation of high-energy phonons). This upconversion of the transmitted phonons is also compared with NE phonons in a bulk solid (native phonons) through heat flux. We use the Ge/Si junction as an example, establish the method and calculations of phonon interaction kinetics from the first principles, describe the need for NE populations and the role of heterojunctions in providing them, and define the process efficiency. NE phonon populations and their interaction kinetics have been extensively studied in phonon transport [13,14]. Since the objective has been relaxation time related to phonon scattering (resistance), rather than energy conversion among phonon modes, the detailed NE population distribution need not be addressed. To our best knowledge, this study is the first on relaxation processes with separate consideration of up- and downconversions and estimation and manipulation of the NE phonon population distribution.

II. UPCONVERSION KINETICS

The potential energy in the crystal Hamiltonian [$H = \langle \varphi \rangle + \sum_i (\mathbf{p}_i^2 / 2M_i)$, where $\sum_i (\mathbf{p}_i^2 / 2M_i)$ is the total kinetic energy (i, atomic index; M_i, mass; $\mathbf{p}_i$, momentum)] is considered for the phonon properties and interaction kinetics and expressed

_____
[*]sshin@utk.edu

as [3,4]

$$\langle\varphi\rangle = \langle\varphi\rangle_{\rm o} + \frac{1}{2!}\sum_{ijxy}\Gamma_{ij}^{xy}d_i^x d_j^y + \frac{1}{3!}\sum_{ijkxyz}\Psi_{ijk}^{xyz}d_i^x d_j^y d_k^z + \dots,$$

(1)

where $\langle\varphi\rangle_{\rm o}$ is the equilibrium potential energy, d_i^x is the displacement of atom i (or j,k) in the x (or y,z) coordinate (Cartesian), and Γ and Ψ are the second- and third-order (cubic) force constants.

Phonons are identified with the wave vector κ [in the first Brillouin zone (BZ)] and mode α, and their energy ($E_{p,\kappa\alpha}$) and crystal momentum ($\mathbf{p}_{p,\kappa}$) are, respectively, $\hbar\omega_{\kappa\alpha}$ and $\hbar\kappa$, where $\hbar$ is the reduced Planck constant and $\omega_{\kappa\alpha}$ is the angular frequency of phonon $\kappa\alpha$. For the phonon energy or frequency with respect to κ and α, we employ the equation of motion for a plane wave using the dynamical matrix $\mathbf{D}$:

$$\omega_\kappa^2 \mathbf{e}_\kappa = \mathbf{D}(\kappa)\mathbf{e}_\kappa.$$

(2)

Here, an element $D_{ij}^{xy}(\kappa)$ of $\mathbf{D}(\kappa)$ is calculated using the second derivatives,

$$D_{ij}^{xy}(\kappa) = \frac{1}{(M_i M_j)^{1/2}}\sum_m \Gamma_{il,jm}^{xy}\exp[i\kappa\cdot(\mathbf{r}_{jm}-\mathbf{r}_{il})],$$

(3)

where M_i is the atomic mass of the ith atom, $\Gamma_{il,jm}^{xy}$ is the second-order force constant of the interaction between the ith atom in the lth unit cell and the jth atom in the mth unit cell, and $\mathbf{r}_{jm}$ is the position vector of the jth atom in the mth unit cell. The phonon angular frequency is obtained from the eigenvalue in Eq. (2), and the number of modes depends on the matrix dimension. Both Ge and Si, considered here, have six phonon modes due to the two atoms in the primitive cell, i.e., longitudinal acoustic (LA), two transverse acoustic (TA1 and TA2; $E_{p,\rm TA1} < E_{p,\rm TA2}$), longitudinal optical (LO), and two transverse optical (TO1 and TO2; $E_{p,\rm TO1} < E_{p,\rm TO2}$).

The kinetics of p-p interactions are studied with the anharmonic (greater than second-order) terms in Eq. (1), and among the interactions, the three-phonon up- and down-conversions depend on the cubic force constants. Higher-order interactions have also been considered [15–18], but the interaction rate decreases as the order increases. The four-phonon interaction rates are negligible compared to three-phonon interactions [17], so the phonon relaxation time is primarily that of three-phonon interactions (although the quartic terms can affect the shift in phonon frequency) [18]. The four possible interactions involving phonon $\kappa\alpha$ are shown in Fig. 1, and through interaction with $\kappa'\alpha'$ and $\kappa''\alpha''$, phonon $\kappa\alpha$ is created (A and B) or annihilated (C and D), conserving the energy and crystal quasimomentum (with transitional invariance [19]).

The three-phonon interaction rate of phonon $\kappa\alpha$ (per primitive cell per second), from the Fermi golden rule [20], is

$$\dot\gamma_{\kappa\alpha} = \sum_{\alpha'\alpha''}\frac{\hbar\pi}{16}\iint_{\rm BZ}\left|\Psi_{\alpha\alpha'\alpha''}^{\kappa\kappa'\kappa''}\right|^2\Delta_{\kappa\kappa'\kappa''}\delta(\omega_{\kappa\alpha},\omega_{\kappa'\alpha'},\omega_{\kappa''\alpha''}),$$

$$\times f_{\rm pop}(f_{p,\kappa\alpha}, f_{p,\kappa'\alpha'}f_{p,\kappa''\alpha''}){\rm d}\kappa'{\rm d}\kappa''.$$

(4)

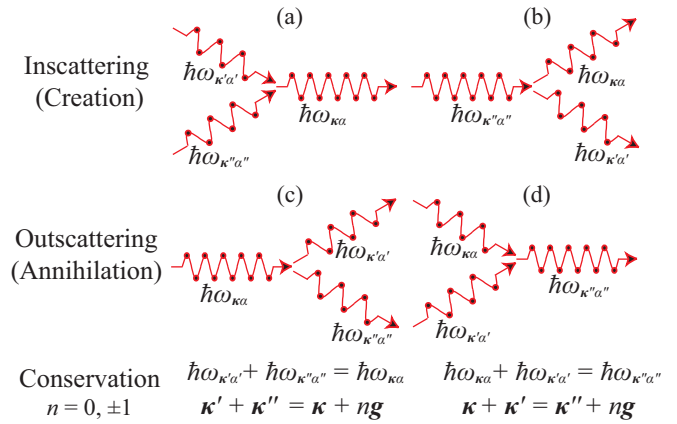For phonon with a wavevector κ and mode α

FIG. 1. (Color online) Three-phonon processes involving a phonon of wave vector κ and mode α interacting with $\kappa'\alpha'$ and $\kappa''\alpha''$, where $\kappa\alpha$ is created (a and b) or annihilated (c and d), with energy and momentum ($\mathbf{g}$ is reciprocal lattice vector) conservations.

Here, the three-phonon interaction element $\Psi_{\alpha\alpha'\alpha''}^{\kappa\kappa'\kappa''}$ is given by [20]

$$\Psi_{\alpha\alpha'\alpha''}^{\kappa\kappa'\kappa''} = \sum_{ijk}\sum_{xyz}\frac{\varepsilon_{xi}^{\kappa\alpha}\varepsilon_{yj}^{\kappa'\alpha'}\varepsilon_{zk}^{\kappa''\alpha''}}{(M_i M_j M_k \omega_{\kappa\alpha}\omega_{\kappa'\alpha'}\omega_{\kappa''\alpha''})^{1/2}}$$

$$\times \Psi_{ijk}^{xyz}\exp\left[i(\kappa\cdot\mathbf{r}_i + \kappa'\cdot\mathbf{r}_j + \kappa''\cdot\mathbf{r}_k)\right],$$

(5)

where $\varepsilon_{xi}^{\kappa\alpha}$ is component x of eigenvector $\mathbf{e}_\kappa$ [from Eq. (2)] for mode α and atom i, and Ψ_{ijk}^{xyz} is the third-order derivatives in Eq. (1). $\Delta_{\kappa\kappa'\kappa''}$ ensures momentum conservation and is unity when $(\kappa - \kappa' - \kappa'')$ for interactions A and C or is 0 or $\pm\mathbf{g}$ (reciprocal lattice vector) when $(\kappa + \kappa' - \kappa'')$ for interactions B and D in Fig. 1; otherwise, it is 0. $\delta(\omega_{\kappa\alpha},\omega_{\kappa'\alpha'},\omega_{\kappa''\alpha''})$ is a delta function of the angular frequency change ($|\omega_{\kappa\alpha} - \omega_{\kappa'\alpha'} - \omega_{\kappa''\alpha''}|$ for A and C, $|\omega_{\kappa\alpha} + \omega_{\kappa'\alpha'} - \omega_{\kappa''\alpha''}|$ for B and D) and is treated with the adaptive broadening scheme [21]. $f_{p,\kappa\alpha}$ is the occupancy of phonon $\kappa\alpha$, and $f_{\rm pop}(f_{p,\kappa\alpha}, f_{p,\kappa'\alpha'}, f_{p,\kappa''\alpha''})$ is the product of $f_{p,\kappa\alpha({\rm or}\ \kappa'\alpha',\kappa''\alpha'')}$ (annihilation) or $f_{p,\kappa\alpha({\rm or}\ \kappa'\alpha',\kappa''\alpha'')} + 1$ (creation) [e.g., for process A, $f_{\rm pop} = (f_{p,\kappa\alpha} + 1)f_{p,\kappa'\alpha'}f_{p,\kappa''\alpha''}$], so the up- and downconversion rates are the same under equilibrium occupancies {Bose-Einstein $f_{p,\kappa\alpha}^{\rm o}(\omega_{\kappa\alpha},T) = [\exp(\hbar\omega_{\kappa\alpha}/k_{\rm B}T) - 1]^{-1}$; $k_{\rm B}$, Boltzmann constant; T, temperature}. In numerical integration of kinetics, we use a Monkhorst-Pack $27 \times 27 \times 27$–point grid (560 points, representing 19 683 points in the first BZ) [22].

The dynamical (or second-order) and the third-order force constant matrices are calculated using the density functional perturbation theory (DFPT) [23] with the first-order perturbation (by the $2n + 1$ formula [24]). The structure relaxation and the unperturbed electron wave-function calculations using the density functional theory (DFT) precede the phonon calculations. The Quantum Espresso package with the norm-conserving pseudopotential in the Perdew-Zunger local density approximation is employed for these DFT and DFPT calculations [25].
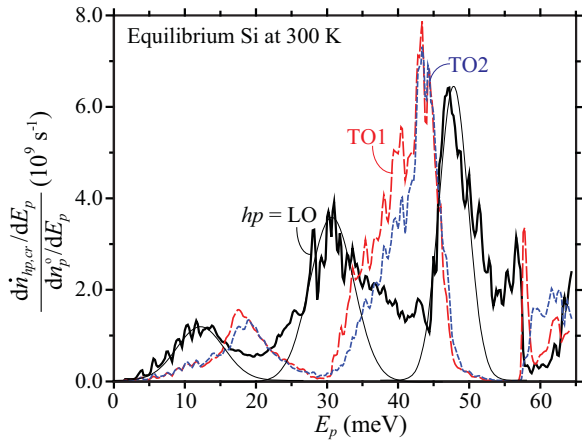
FIG. 2. (Color online) Si optical-phonon creation rates in interaction with an equilibrium phonon of energy E_p, at 300 K (for created phonons hp = LO, TO1, and TO2). Rates (per unit time per unit energy in a primitive cell) are normalized using the equilibrium population distribution dn_p^o/dE_p.

The creation (cr)/annihilation (an) rate of a specific phonon harvested phonon (hp) is calculated by integrating the change rate of the hp population during $\kappa\alpha$-phonon interactions [Eq. (4)] over all wave vectors (κ) and modes (α). The net rate of change of the phonon hp population $\dot{n}_{hp}$ and the energy $\dot{s}_{hp}$ per unit volume are

$$\dot{n}_{hp} = \dot{n}_{hp,cr} - \dot{n}_{hp,an} = \frac{1}{8\pi^3} \sum_s \sum_\alpha \int_{BZ} \dot{\gamma}_{\kappa\alpha,s} \Delta_{\kappa\alpha,hp,s} d \quad \text{and}$$

$$\dot{s}_{hp} = \dot{s}_{hp,cr} - \dot{s}_{hp,an} = \frac{1}{8\pi^3} \sum_s \sum_\alpha \int_{BZ} \dot{\gamma}_{\kappa\alpha,s} \Delta_{\kappa\alpha,hp,s} \hbar\omega_{hp} d\kappa,$$

(6)

where s is process A, B, C, or D, and $\Delta_{\kappa\alpha,hp,s}$ is the population change of hp phonons during process s involving phonon $\kappa\alpha$ (1 or -1). The creation rate is estimated by integrating the interaction rate when $\Delta_{\kappa\alpha,hp,s} = 1$ (for phonon hp annihilation, $\Delta_{\kappa\alpha,hp,s} = -1$), and the net change in hp results from upconversion of low-energy acoustic phonons and downconversion to two acoustic phonons. Under equilibrium, the net population change of the LO, TO1, or TO2 is 0 (based on the principle of detailed balance [26]), although the creation and annihilation rates are nonzero (e.g., $\dot{n}_{LO,cr} = \dot{n}_{LO,an} = 5.77 \times 10^{-8}$ s^{-1} per primitive cell at 300 K), and the net creation requires an NE distribution with underpopulation of a targeted mode or overpopulation of other modes.

To identify phonons most effective for upconversion, the spectral contribution to phonon creation/annihilation rates for hp are calculated by projection of the rates for phonons with energy E_p and shown in Fig. 2 under equilibrium at 300 K. Since the spectral contribution $d\dot{n}_{hp,cr(or an)}/dE_p$ is larger in energy with a larger population, we normalize it with the population distribution (dn_p^o/dE_p) to identify the single-phonon contribution. Under equilibrium, creation and annihilation are balanced, so only the creation rate is shown in Fig. 2. The results suggest that when overpopulated, 12-, 30-, and 48-meV phonons are effective in LO phonon creation and

19-, 40-, and 44-meV phonons in TO phonon creation (results for TO1 and TO2 phonons are similar). The creation of these overpopulations is discussed next with the introduction of the HPUC.

III. NONEQUILIBRIUM POPULATION

As discussed, overpopulation of low-energy phonons [or underpopulation of high-energy (optical) phonons] is required for net upconversion, and careful selection of these overpopulated modes leads to optimal conversion to targeted phonons. Although NE occupancies ($f_p \neq f_p^o$) are formed under energy conversion and transport, these population deviations are not significant unless there is a transport with a large temperature gradient or a high-energy injection in a short time [27]. To control distinct phonon nonequilibria, we introduce a heterojunction where the contrast (mismatch) of phonon states results in junction (interface) reflections and local nonequilibria in interfacial regions (although semiclassical treatments of interfacial phonon transport simply assume equilibrium, as discussed in [28] and [29]).

At a given atomic density, a soft solid with a lower Debye temperature has a larger population of low-energy phonons compared to a hard solid (including its optical modes). Thus, in phonon transport from soft to hard material, the upconversion-favorable, low-energy phonon modes are more populated in the adjacent hard layer compared to phonon transport in a homogeneous hard solid. We employ Ge as a soft semiconductor solid, and Si as a hard one, and study phonon transport across a Ge/Si bilayer and transported phonon harvesting (absorption) in Si in an energy conversion process.

For a Ge/Si heterostructure the phonon properties and upconversion processes are depicted in Fig. 3(a). With the same atomic structure (diamond cubic) and similar lattice constants (Ge, 5.65 Å; Si, 5.43 Å) [30], their phonon dispersion and density of states ($D_{p,Ge}$ and $D_{p,Si}$) are similar with six phonon modes (the transverse modes are degenerated in Γ–X). However, the larger atomic mass and weaker interatomic force field result in a larger population of low-energy phonons in Ge. Under phonon flux q_p (temperature gradient), Ge phonons across the heterojunction create an overpopulation of low-energy acoustic Si phonons (Ge, i.e., transmitted phonons) near the interface. These overpopulated phonons are upconverted to Si optical modes and harvested (or otherwise downconverted by thermalization).

Phonons in Ge and Si are relaxed within a few hundred nanometers [31] from the interface, and also any atomic restructuring in the interfacial region does not extend beyond a few nanometers [29,32]. So, over a distance of $O(100 \text{ nm})$ from the interface the phonons are relaxed to the equilibrium occupancy. Under thermal energy flux q_p, the phonon temperature T_p (or population f_p) increases compared to the initial equilibrium temperature, with the temperature gradient (spatial distribution of the phonon population) depending on the transport property. With the high thermal conductivity of Ge and Si ($k_{Ge} = 60$ and $k_{Si} = 148$ W/m-K at 300 K [33]) and their interfacial phonon conductance ($G_{b,Ge/Si}/A = 0.75$ GW/m^2-K [31]), unless the phonon flux is extremely high (>7.67 kW/cm^2), the temperature variation over a distance
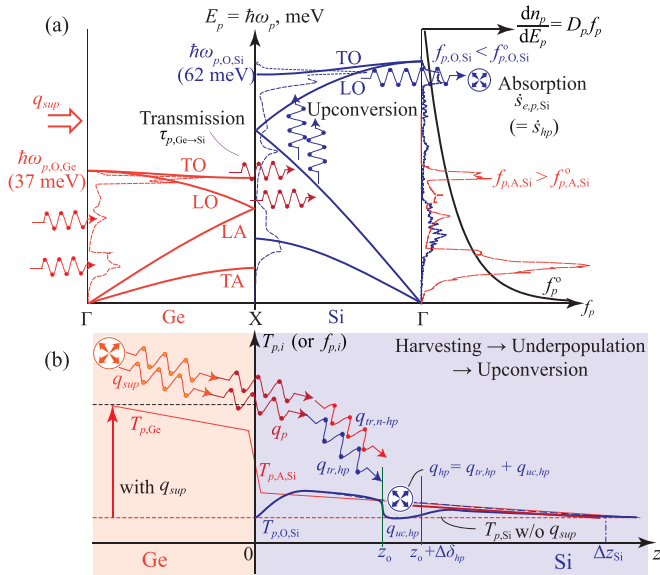
FIG. 3. (Color online) Schematics of phonon harvesting at the Ge/Si heterojunction (HPUC). (a) Phonon dispersion, density of states (D_p), and population distribution for Ge and Si. Under flux, due to the larger D_p at Ge acoustic and optical modes, low-energy phonons in Si are overpopulated and then upconverted to Si optical phonons. (b) Anticipated spatial distributions of the optical and acoustic phonon temperatures ($T_{p,O}$ and $T_{p,A}$ with an interfacial temperature drop due to boundary resistance). The phonon source is in Ge and the phonon flux in the z direction creates the temperature variations in Si. The Si optical mode is less populated, because none is transmitted from Ge. The targeted phonon mode (hp) is harvested (absorbed by the other system) in $[z_o, z_o + \Delta\delta_{hp}]$, and this leads to the underpopulation. The harvested phonon flux q_{hp} is due to transport of harvested ($q_{tr,hp}$)–mode and conversion of nonharvested (nhp)–mode phonons ($q_{up,hp}$).

of $O(100$ nm$)$ on both sides of the interface is negligible (<1 K, within 1-μm interfacial region) [using the total thermal resistance ($AR_{Ge/Si} = AR_{k,Ge} + AR_{b,Ge/Si} + AR_{k,Si} = l/k_{Ge} + A/G_{b,Ge/Si} + l/k_{Si} = 130$ μK-cm^2/W, where $l = 0.5$ μm)]. We consider heterojunction upconversion within a length of $O(100$ nm$)$ from the interface and a phonon flux of less than 7.67 kW/cm^2, so the temperature change over the interested heterostructure region is negligible. The phonon population change due to this heat flux is not significant after relaxation, and phonons upstream (before transmission across the heterojunction) are assumed to be in equilibrium.

With phonon flux from the Ge layer, the spatial distributions of the anticipated optical and acoustic phonon temperatures in the HPUC system are shown in Fig. 3(b). Since the Ge-transmitted phonons are not populated in the Si-optical mode range, the optical temperature at the interface is not increased by the phonon flux. However, as the transmitted acoustic phonons are upconverted (relaxed), the optical phonon temperature follows the acoustic counterpart. If we harvest optical phonons (absorbed by the other system) in $[z_o, z_o + \Delta\delta_{hp}]$ ($\Delta\delta_{hp}$ is the length of the phonon-harvesting region), the harvested phonon mode (hp) is underpopulated (lower phonon temperature) and enhances the upconversion. Thus, the harvested (or absorbed) phonons can be supplied by conversion of nonharvested (nhp)-mode photons as well as

transport of harvested-mode (hp) phonons (created between the interface and the harvested site).

The equilibrium population distributions are calculated using the equilibrium occupancy function f_p^o and the phonon density of states D_p calculated from the DFPT, i.e., $dn_p^o/dE_p = D_p f_p^o$, and the results for Ge and Si are shown in Fig. 4(a) for 300 K. To predict the distribution of Ge/Si heterojunction-transmitted phonons, the spectral phonon junction transmission from Ge to Si $\tau_{p,Ge\to Si}(E_p)$ and the Ge equilibrium distribution $dn_{p,Ge}^o/dE_p$ are used. The transmitted distribution in the Si layer is estimated as $dn_p/dE_p|_{z=+0} = \tau_{p,Ge\to Si}dn_{p,Ge}^o/dE_p$ (interface at $z = 0$), and these phonons originating from the Ge layer are called Ge-transmitted phonons, compared with Si-native phonons.

The nonequilibrium Green function (NEGF) formalism [34] provides the spectral transmission used in prediction of the NE phonon distribution. In NEGF calculations, the interface is a scattering region, with the two sides having equilibrium populations away from this interface (reservoirs not affected by the transport). Phonon transmission across the interface represents scattering by the interfacial-region structure, and transmitted phonons will be further relaxed through p-p interactions. All the functions required in the NEGF are calculated using the force-constant matrices of the heterojunction. Among them, the self-energy [$\boldsymbol{\Sigma}_L^r$ or $\boldsymbol{\Sigma}_R^r$, where the superscript r represents retarded, as opposed to advanced (a), and the subscripts L and R represent left and right] represents the interaction of semi-infinite Ge and Si layers (slabs) with the heterojunction and is calculated employing the decimation technique [35]. Using the self-energy, the phonon retarded Green function is given by [36]

$$\mathbf{G}^r = [(\omega + i\eta)^2 \mathbf{I} - \mathbf{K}_{CC} - \boldsymbol{\Sigma}_L^r - \boldsymbol{\Sigma}_R^r], \tag{7}$$

where $\mathbf{I}$ is the identical matrix, $\mathbf{K}_{CC}$ is the force constant matrix of the heterojunction at the center, ω is the angular frequency of the phonon, and η is an infinitesimal number for the phonon energy dissipation [37]. Then the phonon transmission across the heterojunction is [38,39]

$$\tau_p = \text{Tr}[\boldsymbol{\Gamma}_L \mathbf{G}^r \boldsymbol{\Gamma}_R \mathbf{G}^a], \tag{8}$$

where $\mathbf{G}^a$ is the phonon advanced Green function equivalent to $(\mathbf{G}^r)^\dagger$ and $\boldsymbol{\Gamma}_L (\boldsymbol{\Gamma}_R)$ is the energy-level broadening function caused by the left (right) contact and described by $\boldsymbol{\Gamma}_{L/R} = i(\boldsymbol{\Sigma}_{L/R}^r - \boldsymbol{\Sigma}_{L/R}^a)$.

We employed the NEGF spectral transmission [using the right axis in Fig. 4(a)] of the Ge/Si heterojunction from Ref. [40], where the force constant matrices are calculated using the many-body Tersoff potential [41] and an ideal (perfectly smooth) interface is assumed. (The results from Ref. [40] agree well with other reports [42,43].) The atomic roughness affects the interfacial phonon scattering depending on the phonon wavelength (or frequency) and the incident angle [42]. Depending on the atomic configuration, well-controlled roughness can increase the transmission (especially at a midrange frequency) by smoothing the abrupt acoustic impedance mismatch and increase in interfacial area [44]. Thus, the NE phonon distribution can be further tuned using the interfacial atomic roughness. Also, since the harmonic (second-order) force constants are used in the Green function
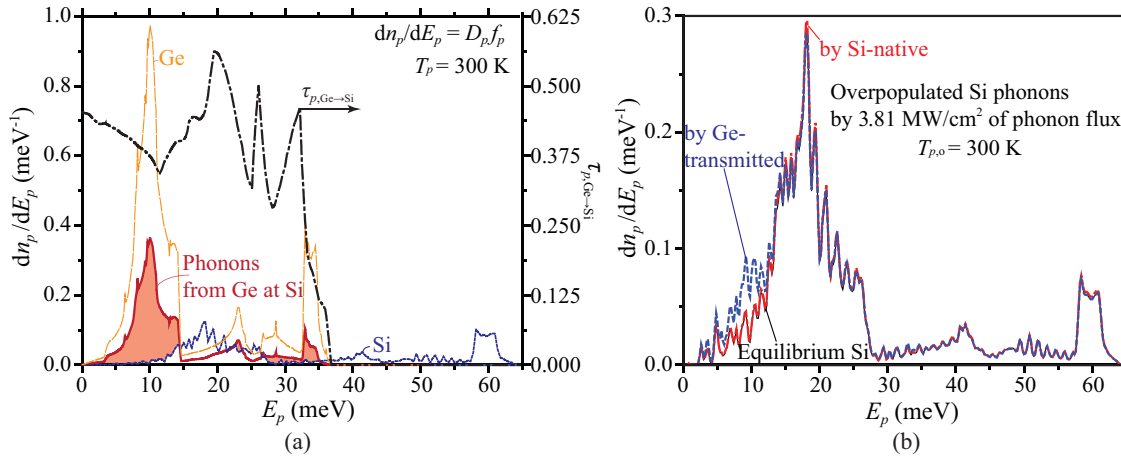
FIG. 4. (Color online) (a) Phonon population (per primitive cell) distributions adjacent to junctions, based on the NEGF transmission spectrum [40] for Ge/Si phonons (right axis), at 300 K. Shaded regions represent larger overpopulation by transmitted Ge phonons. Si and Ge equilibrium distributions are also shown for contrast. (b) Nonequilibrium phonon distribution created by Ge-transmitted and Si-native phonons under the same phonon flux (3.8 MW/cm²). Si phonon modes matching the Ge phonons are more pronouncedly overpopulated by the Ge-transmitted phonon flux.

calculation, anharmonic effects are excluded in this transmission (anharmonicity can be included in the NEGF [45]).

The transmitted Ge phonon distribution at the Si-side interface calculated using the NEGF transmission is shown in Fig. 4(a), and its occupancy in Si is NE ($f_{p,\text{Ge/Si}} = \tau_{p,\text{Ge}\to\text{Si}} D_{p,\text{Ge}} f_p^o / D_{p,\text{Si}}$, where the subscript Ge/Si is for Ge-transmitted phonons in Si). Through this heterojunction transport with nonunity spectral transmission, Si phonons in ranges of [0, 14.5 meV] and [26, 35 meV] are overpopulated, and these phonons are effective to create Si LO phonons according to the results shown in Fig. 2. The phonons, transported from Ge to Si, eventually relax to the Si phonon equilibrium population, but the transported phonon distribution remains deviated from equilibrium until fully relaxed, and this deviation is the most prominent adjacent to the interface. In particular, those Si phonon modes matching the Ge phonons are pronouncedly more overpopulated compared to the equilibrium population.

The transmitted Ge phonons are added to the equilibrium population of Si, and this NE contribution increases with the phonon flux q_p. In addition, we impose optical phonon harvesting in the Si layer, and this is done by maintaining the population of Si optical phonons. For steady phonon harvesting, we balance the Si optical phonons created by the Ge phonon transmission with the harvesting (absorption) of these Si optical phonons, so here the population of harvested phonons is assumed to be in equilibrium, while allowing for the overpopulation of the Ge-transmitted modes. The nonharvested (nhp; acoustic in Si) modes are overpopulated by the transmitted phonons ($f_{p,\kappa\alpha} > f_{p,\kappa\alpha}^o$), and these NE phonons in transit contribute to the phonon flux as [3]

$$\mathbf{q}_p = \frac{1}{8\pi^3} \sum_\alpha \int_{\text{BZ}} f'_{p,\kappa\alpha} \mathbf{u}_{p,\kappa\alpha} \hbar\omega_{p,\kappa\alpha} d\kappa, \qquad (9)$$

where $f'_{p,\kappa\alpha}$ is the occupancy deviation from equilibrium of phonon $\kappa\alpha$ ($f_{p,\kappa\alpha} - f_{p,\kappa\alpha}^o$), and $\mathbf{u}_{p,\kappa\alpha}$ is the phonon velocity. Here, the deviation originates from the overpopulated phonons propagating in the transport direction ($f'_{p,\kappa\alpha} = f_{p,\kappa\alpha}^+$).

To study the upconversion effectiveness of the HPUC structure, the overpopulation distributions by the Ge-transmitted (across the Ge/Si heterojunction) and the Si-native phonon fluxes are considered, and the former is only observed near the interface in the Si layer, while the latter persists sufficiently far from the interface. The overpopulated phonon populations are estimated as a fraction of the Ge-transmitted phonons and equilibrium Si phonons in Fig. 4(a); i.e., $f_p^+ = a f_{p,\text{Ge/Si}}$ and $b f_{p,\text{Si}}^o$, with a and b as constants, where subscripts Ge/Si and Si stand for Ge-transmitted and Si-native, respectively. The overpopulated energy in the primitive cell is $\langle E_p^+ \rangle = \int D_p f_p^+ dE_p$, and using Eq. (9) and the spectral mode-average velocities from Ref. [46], we have $q_p = (1.27 \text{ kW/cm}^2\text{-}\mu\text{eV})\langle E_{p,\text{Ge/Si}}^+ \rangle$, where $\langle E_{p,\text{Ge/Si}}^+ \rangle$ is the overpopulated Ge-transmitted phonon energy in the primitive cell. The native-Si phonon overpopulation $\langle E_{p,\text{Si}}^+ \rangle$ with the same q_p is used as the benchmark. Since high-speed, low-energy phonons are less populated in Si-native phonons than Ge-transmitted phonons, $\langle E_{p,\text{Si}}^+ \rangle$ is larger than $\langle E_{p,\text{Ge/Si}}^+ \rangle$ for the same q_p.

The NE population distribution is $dn_p/dE_p = D_p(f_{p,\text{Si}}^o + f_p^+)$, while the harvested-mode population remains at equilibrium. Figure 4(b) shows the transmission-induced population increase and deviation from the equilibrium distribution. We also show the imposed uniform overpopulation of the Si-native phonon used in the phonon upconversion under the same phonon flux. Here the overpopulation is added to the Si equilibrium phonon distribution ($f_{p,\text{Si}}^o$) at 300 K. For more a pronounced deviation, the overpopulated distributions under the very high phonon flux of 3.8 MW/cm² (which induces 3 meV overpopulation per primitive cell for Ge-transmitted phonons) are shown in Fig. 4(b).

This NE can be observed by measuring the phonon optical properties or analyzing the atomic vibration simulations such as *ab initio* or classical molecular dynamics. Ge phonons transmitted to the Si layer, i.e., undergoing filtering, change the local phonon population in Si and this can be measured to confirm the NE population a short distance from the interface. Phonons, having a high momentum and relatively

low energy, assist in photon-matter interactions [47,48], so the larger the phonon population, the higher the photon absorption/emission rate [49]. NE phonons are also observed with x-ray methods, e.g., x-ray scattering, which is sensitive to short-wavelength phonons, which reduce the intensity of Bragg peaks and produce a diffuse scattering background [50]. Also, time-resolved anti-Stokes Raman scattering can measure the population change [51–53]. In addition to experiments, the change in the phonon population distribution can be simulated with molecular dynamics (classical [54] and *ab initio* [55]) and analysis of local atomic displacements.

IV. UPCONVERSION EFFICIENCY

Under NE, the optical-mode creation and annihilation rates are no longer balanced. Using the NE distributions by the Ge-transmitted and the Si-native phonon fluxes for the heat flux $q_p = 1.27$ kW/cm^2, where $\langle E_{p,\text{Si}}^+ \rangle = 1.24$ μeV and $\langle E_{p,\text{Ge/Si}}^+ \rangle = 1$ μeV) (for this overpopulation, $a = 3.01 \times 10^{-5}$ and $b = 2.31 \times 10^{-5}$ in $f_p^+ = af_{p,\text{Ge/Si}}$ and $bf_{p,\text{Si}}^o$), the net creation rate for the targeted (harvested) phonon is calculated using Eq. (4). When the Si LO-mode phonons are harvested (hp = LO), the net creation rates by Si-native and Ge-transmitted phonons are $\dot{s}_{\text{LO,Si}} = 1.43$ W/cm^2-nm and $\dot{s}_{\text{LO,Ge/Si}} = 1.33$ W/cm^2-nm. The net creation rate (mainly by upconversion) increases with an increase in q_p (f_p^+ or $\langle E_p^+ \rangle$), and for $q_p < 1$ MW/cm^2, the hp energy generation rate $\dot{s}_{\text{hp}}$ is linearly proportional to q_p. Since both the Ge-transmitted and the Si-native overpopulations are added to the same equilibrium, the spatial temperature variations should be minimized to ignore variation of the equilibrium distribution, and for $q_p < 7.67$ kW/cm^2 in the linear regime of the q_p-$\dot{s}_{\text{hp}}$ relation, we find a variation $\Delta T < 1$ K within 1 μm of the junction region. So, under the linear relation and small-T-variation limit, we normalize $\dot{s}_{\text{hp}}$ with the heat flux q_p and average phonon mean free path λ_p, i.e., $\dot{s}_{\text{hp}}^* = \dot{s}_{\text{hp}}/(q_p/\lambda_p)$. The phonon mean free path ($\lambda_p = 115$ nm) is estimated from the phonon transport properties using the conductivity relation $k_p = nc_v u_p \lambda_p / 3$, where n is the phonon number density, c_v is the specific heat capacity, and the spectral mode-average velocities from Ref. [46] are used for the phonon velocity u_p [3,30]. This gives $\dot{s}_{\text{LO,Si}}^* = 0.127$ and $\dot{s}_{\text{LO,Ge/Si}}^* = 0.121$ at 300 K. For upconversion to the TO1 and TO2 modes, $\dot{s}_{\text{TO1,Si}}^* = 0.173$ and $\dot{s}_{\text{TO1,Ge/Si}}^* = 0.0696$, and $\dot{s}_{\text{TO2,Si}}^* = 0.159$ and $\dot{s}_{\text{TO2,Ge/Si}}^* = 0.0545$. For all three optical modes, the net creation rate by Si-native overpopulated phonons ($f_p^+ = bf_{p,\text{Si}}^o$) is larger than that by NE Ge-transmitted phonons ($f_p^+ = af_{p,\text{Ge/Si}}$) with the same heat flux, and the difference between these two is smallest for the LO-mode upconversion. The $af_{p,\text{Ge/Si}}$ is expected to favor the LO-mode upconversion from Figs. 2 and 4, and these results confirm this.

Depending on the phonon-harvesting system, different phonon wave vectors are required [56], so we study the upconversion to optical phonons with the selected wave vectors. We sample the grid ($V_{\text{BZ}}/19683$; V_{BZ}, first BZ) and the dimensionless, local net creation rate for phonon $\kappa^* \alpha$ per dimensionless reciprocal volume ($\text{d}\dot{s}_{\kappa\alpha}^*/\text{d}\kappa^*$ for hp = $\kappa^* \alpha$) is calculated with respect to the dimensionless wave vector κ^* (normalized by $2\pi/a$; a, lattice constant) with one optical
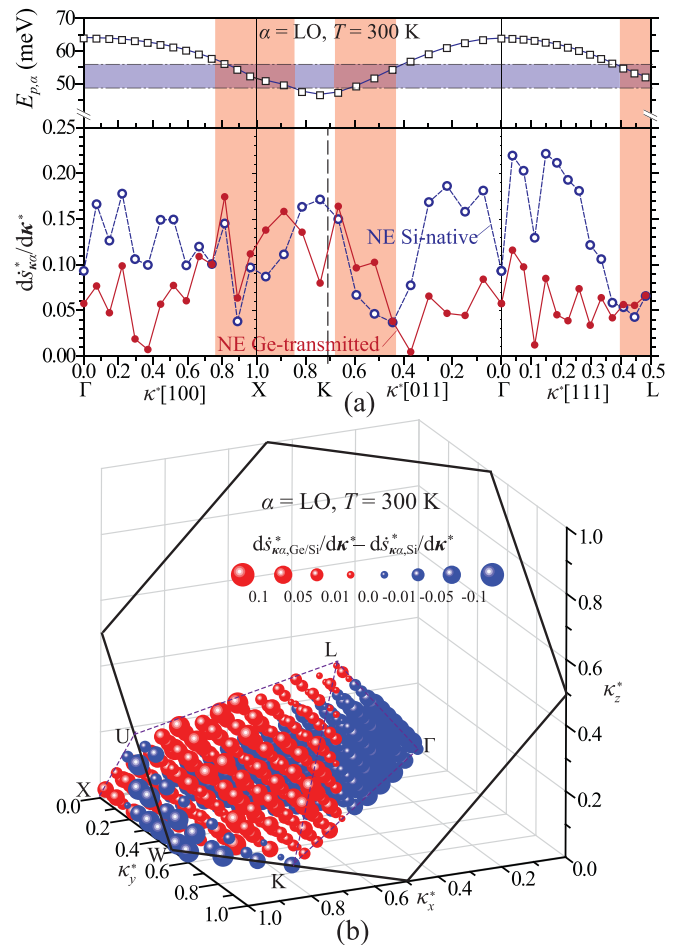

FIG. 5. (Color online) (a) Variations of dimensionless, local net creation (upconversion) rates for LO phonons ($\text{d}\dot{s}_{\kappa\alpha}^*/\text{d}\kappa^*$; $\alpha = $ LO) from Ge-transmitted and Si-native overpopulated phonons, along high-symmetry axes. The created optical phonon energy ($E_{p,\text{LO}}$) is also shown (upper), and it is evident that overpopulation by Ge-transmitted phonons results in a higher LO phonon creation rate in the regime [49, 56 meV] compared to NE Si-native phonons. (b) Difference between $\text{d}\dot{s}_{\kappa\alpha,\text{Si}}^*/\text{d}\kappa^*$ and $\text{d}\dot{s}_{\kappa\alpha,\text{Ge/Si}}^*/\text{d}\kappa^*$ in an irreducible BZ wedge. Spheres are centered at the sampling points of a $27 \times 27 \times 27$ grid, showing the wave vector of the upconverted (harvested) phonon. Red represents a larger $\text{d}\dot{s}_{\kappa\alpha,\text{Ge/Si}}^*/\text{d}\kappa^*$, blue a larger $\text{d}\dot{s}_{\kappa\alpha,\text{Si}}^*/\text{d}\kappa^*$, and the diameter indicates the magnitude. Results are for 300 K.

mode ($\text{d}\dot{s}_{\kappa\alpha}^*/\text{d}\kappa^* = 0$ under equilibrium). We integrate this rate for a selected wave-vector space ($\kappa^* = \kappa_{\text{sel}}^*$), i.e., $\dot{s}_{(\kappa^* = \kappa_{\text{sel}}^*)\alpha}^* = \int_{\kappa^* = \kappa_{\text{sel}}^*} (\text{d}\dot{s}_{\kappa\alpha}^*/\text{d}\kappa^*) \text{d}\kappa^*$.

The dimensionless, local net creation rate for LO phonons ($\alpha = $ LO) is calculated on irreducible κ points in a $27 \times 27 \times 27$ sampling grid for NE Si-native and NE Ge-transmitted prescribed overpopulations and are plotted along high-symmetry axes in Fig. 5(a). The difference between these two rates is also plotted in one irreducible BZ wedge in Fig. 5(b). Both figures show that, overall, NE Ge-transmitted phonons have a smaller $\text{d}\dot{s}_{\kappa\alpha}^*/\text{d}\kappa^*$ when creating LO phonons near Γ [i.e., $\kappa^* = (0,0,0)$] compared to NE Si-native phonons. In addition to the zone center region (Γ), NE Si-native phonons are more effectively upconverted to LO phonons at

the zone boundary κ^* points around the U-W-K line, while NE Ge-transmitted phonons are effective for harvesting LO phonons near the L or X points. Ge-transmitted phonons provide large populations around 10 and 33 meV [Fig. 4(a)], interact with equilibrium (E) Si phonons (peaks near 18 and 42 meV), and effectively upconvert to Si-LO phonons between 49 and 56 meV [especially at 51 (33 + 18) and 52 (10 + 42) meV] [Fig. 5(a)].

In upconverted optical phonon harvesting, the efficiency η_{hp} is defined as the ratio of harvested q_{hp}-to-supplied q_{sup} phonon fluxes (in Ge), $\eta_{\mathrm{hp}} = q_{\mathrm{hp}}/q_{\mathrm{sup}}$, and this includes the junction transmission and upconversion processes. With the heterojunction, q_{sup} in the ballistic regime is predicted from the transmission $\tau_{p,\mathrm{Ge}\rightarrow\mathrm{Si}}$ and actual phonon flux over system q_p, and considering the transmission and phonon flux depending on the wave vector and mode, $q_{\mathrm{sup}} = \sum_\alpha \int_{\mathrm{BZ}} (dq_{\mathrm{sup},\kappa\alpha}/d\kappa^*)d\kappa^* = \sum_\alpha \int_{\mathrm{BZ}} dq_{p,\kappa\alpha}/(\tau_{p,\kappa\alpha,\mathrm{Ge}\rightarrow\mathrm{Si}}d\kappa^*)d\kappa^*$, where $dq_{\mathrm{sup\,(or\,}p),\kappa\alpha}/d\kappa^*$ is the contribution of phonon $\kappa^*\alpha$ to the heat flux $q_{\mathrm{sup\,(or\,}p)}$ (heat flux by phonon $\kappa^*\alpha$ per dimensionless reciprocal volume), and $dq_{p,\kappa\alpha}/d\kappa^* = \tau_{p,\kappa\alpha,\mathrm{Ge}\rightarrow\mathrm{Si}}(dq_{\mathrm{sup},\kappa\alpha}/d\kappa^*)$ in the ballistic regime. At steady state, the harvested phonon flux q_{hp} is balanced by the transported, harvested optical phonon flux $q_{\mathrm{tr,hp}}$ [using Eq. (9) for the hp mode] and the upconverted phonon flux $q_{\mathrm{uc,hp}}$; thus, $q_{\mathrm{hp}} = q_{\mathrm{tr,hp}} + q_{\mathrm{uc,hp}}$. The latter is the integration of the upconversion rate over the phonon-harvesting region $\Delta\delta_{\mathrm{hp}}$ [in Fig. 2(b)], i.e., $q_{\mathrm{uc,hp}} = \int_{\Delta\delta_{\mathrm{hp}}} \dot{s}_{\mathrm{hp}}dz$.

Since the phonon flux from Ge does not include optical modes (i.e., there is no transported, harvested phonon, $q_{\mathrm{tr,hp}}$) and with the nonunity junction transmission further reducing the flux, a low efficiency is expected for NE Ge-transmitted phonons. This holds even for the Ge-favored upconversion channels (i.e., resulting in $d\dot{s}^*_{\kappa\alpha,\mathrm{Ge/Si}}/d\kappa^* > d\dot{s}^*_{\kappa\alpha,\mathrm{Si}}/d\kappa^*$). As the transported phonon distribution evolves from NE Ge-transmitted to NE Si-native through relaxation, the phonon flux includes the harvested mode ($q_{\mathrm{tr,hp}}$) and the upconversion rate becomes close to the NE Si-native $\dot{s}_{\kappa\alpha,\mathrm{Si}}$.

We calculate the spatial (from the junction) variations of efficiency at selected κ^* points with $\Delta z = \lambda_p/10$ of harvesting bins ($\Delta\delta_{\mathrm{hp}} = \Delta z$). The overpopulation distribution in $0 \leqslant z \leqslant \lambda_p$ is treated as a linear interpolation of the Ge-transmitted and Si-native overpopulations, and the transported $\kappa^*\alpha$ phonon flux $q_{\mathrm{tr},\kappa\alpha}$ and creation rate $\dot{s}_{\kappa\alpha}$ (for selected hp = $\kappa^*\alpha$) follow this variation. Adding the low velocity and short lifetime of the optical phonons (shorter relaxation length), $q_{\mathrm{tr},\kappa\alpha}$ approaches the NE Si-native magnitude more rapidly the than upconverted $\kappa^*\alpha$ phonon flux $q_{\mathrm{uc},\kappa\alpha}$ (and $\dot{s}_{\kappa\alpha}$).

Figure 6 shows the variation of the local harvesting efficiency $d\eta_{\mathrm{hp}=\kappa\alpha}/d\kappa^*$ (using $q_{\kappa\alpha}$ per dimensionless reciprocal volume) for two $\kappa^*\alpha$ values: (i) $\alpha = \mathrm{LO}$ and $\kappa^* = (0.81, 0.52, 0.07)$, which is more effectively upconverted by Ge-transmitted compared to Si-native phonons, $d\dot{s}^*_{\kappa\alpha,\mathrm{Ge/Si}}/d\kappa^* > d\dot{s}^*_{\kappa\alpha,\mathrm{Si}}/d\kappa^*$; and (ii) $\alpha = \mathrm{LO}$ and $\kappa^* = (0.15, 0.15, 0.15)$, where $d\dot{s}^*_{\kappa\alpha,\mathrm{Ge/Si}}/d\kappa^* < d\dot{s}^*_{\kappa\alpha,\mathrm{Si}}/d\kappa^*$. For the first κ^*, an optimal (not that pronounced) location for harvesting ($\delta_{\mathrm{hp}=\kappa\alpha,\mathrm{max}}$) exists before the relaxation. For the second κ^*, both $q_{\mathrm{tr},\kappa\alpha}$ and $q_{\mathrm{uc},\kappa\alpha}$ increase as the flux is relaxed and the local harvesting efficiency $d\eta_{\mathrm{hp}=\kappa\alpha}/d\kappa^*$ increases monotonically. So, depending on the $q_{\mathrm{tr},\kappa\alpha}$ variation, which can dominate over variation of $q_{\mathrm{uc},\kappa\alpha}$, $\delta_{\mathrm{hp}=\kappa\alpha,\mathrm{max}}$ can be larger than λ_p. The bulk Si and the fully relaxed region in Ge/Si ($z > \lambda_p$)
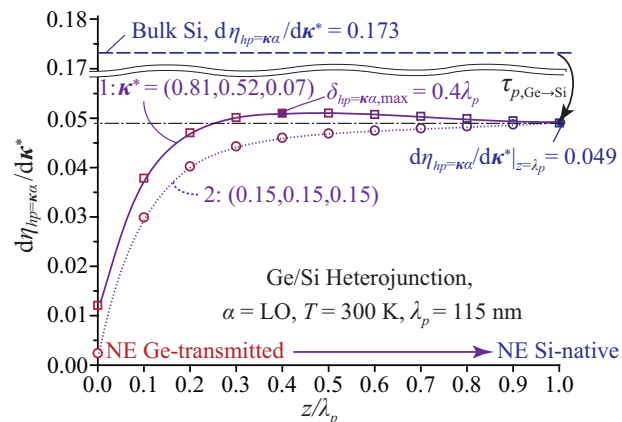

FIG. 6. (Color online) Spatial variations of the local harvesting efficiency ($d\eta_{\mathrm{hp}=\kappa\alpha}/d\kappa^*$) for two wave vectors, $\kappa^* = (0.81, 0.52, 0.07)$ near the zone boundary (solid line) and $(0.15, 0.15, 0.15)$ near the zone center (dotted line). For the first, the optimal location for efficiency (filled square) exists before relaxation, while for the second the efficiency increases monotonically. $d\eta_{\mathrm{hp}=\kappa\alpha}/d\kappa^*$ in bulk Si (dashed line) is larger with no loss by heterojunction transmission ($\tau_{p,\mathrm{Ge}\rightarrow\mathrm{Si}}$).

have the same overpopulation and $q_{\kappa\alpha}$ with a given q_p, but in bulk Si q_{sup} is smaller by $\tau_{p,\mathrm{Ge}\rightarrow\mathrm{Si}}$ and $d\eta_{\mathrm{hp}=\kappa\alpha}/d\kappa^*$ is larger than the Ge/Si structure as shown in Fig. 6. Thus, compared to native phonons in bulk Si, the overall harvesting efficiency η_{hp} for the transmitted phonons is lower, because of the interfacial reflection, even though the upconversion efficiency excluding the phonon supply by transport; i.e., $\eta_{\mathrm{uc,hp}} = q_{\mathrm{uc,hp}}/q_{\mathrm{sup}}$, is higher for NE Ge-transmitted phonons. As phonons are harvested and the phonon flux is reduced (the harvesting site is located adjacent to the interface and within the relaxation length), this phonon flux reduction depends on the phonon flow direction (i.e., flowing from the soft to the hard solid, or vice versa). This is due to the distinct NE phonon populations on the two sides. This directional dependency is a thermal rectification [57] and its magnitude depends on the harvested phonon mode and location, as shown in Fig. 6.

V. CONCLUSIONS

In the quest to increase the solid-state energy conversion efficiency, resonant phonons may be targeted for harvesting instead of heat (equilibrium phonon occupancy). These NE phonons may be available as a result of local emission (including nonradiative decay) but may also be created by *p*-*p* interactions. For effective supply of the energetic optical (resonant) phonons, the *p*-*p* interaction kinetics and the NE phonon distribution are controlled by the heterojuction transmission. Here we have compared the effectiveness of NE native and heterojunction (soft/hard bilayer)–transmitted phonons for upconversion to optical phonons, addressed the related phonon physics and interaction kinetics, defined upconversion efficiency, and made specific calculations for the Ge/Si bilayer. The creation and annihilation rates of Si optical phonons are calculated using the third-order force constants from DFPT, and the effective phonons for creating the targeted optical modes are identified (12-, 30-, and 48-meV phonons for LO phonon creation and 19-, 40-, and 44-meV

phonons for TO phonon creation). The NE distribution by heterojunction-transmitted phonons is estimated using the spectral transmission (from NEGF), and it is shown that the Ge-transmitted phonons create large populations of the low-energy acoustic and the Ge optical modes, which are effective in the creation of Si LO phonons (for harvesting absorption). Ge-transmitted and Si-native phonons have their distinct high upconversion efficiency regions in the BZ, which can be targeted for harvesting. For example, since Si is an indirect-gap semiconductor [valence band at and conduction band near the X point (multiple locations)], phonons near the zone boundary are harvested through phonon-assisted, photon absorption processes [58]. Here we show that Ge-transmitted phonons can also create/supply these phonons (Ge-transmitted phonons are effective for zone-boundary phonons near the L and X points, and Si-native phonons for other regions).

Substituting Ge with another soft solid, for example, InP, which has the optical mode at 42 meV [59], can be more effective for Si TO phonon creation, as suggested by Fig. 2. Also, using the alloy Si_xGe_{1-x}, which has an additional optical mode at 50 meV (for LO phonon creation), allows for resonant, high-upconversion-efficiency selection by choosing the Si content x [60]. Energy conversion among the NE phonon modes leads to fundamental improvements in resonant phonon harvesting, including thermal rectification, which accompanies phonon-flux-direction-dependent phonon harvesting, and IR photon emission through absorption of optical phonons. Traditionally, phonons are regarded as energy dissipation agents or parasite interferers with electron transport; however, with the control of the phonon population distribution and the related interaction kinetics, as suggested here, harvesting of resonance phonons as an energy source can evolve phonon research and phononic applications [61,62].

ACKNOWLEDGMENTS

[1] M. Lundstrom, *Fundamentals of Carrier Transport* (Cambridge University Press, New York, 2000).

[2] R. D. Mattuck and M. W. P. Strandberg, Spin-phonon interaction in paramagnetic crystals, Phys. Rev. **119**, 1204 (1960).

[3] M. Kaviany, *Heat Transfer Physics*, 2nd ed. (Cambridge University Press, New York, 2014).

[4] G. P. Srivastava, *The Physics of Phonons* (Adam Hilger, Bristol, UK, 1990).

[5] M. Haase and H. Schäfer, Upconverting nanoparticles, Angew. Chem. Int. Ed. **50**, 5808 (2011).

[6] F. Auzel, Upconversion and anti-Stokes processes with f and d ions in solids, Chem. Rev. **104**, 139 (2003).

[7] H. U. Güdel, New light-emitting inorganic materials, Chimia **52**, 561 (1998).

[8] S. Shin, C. Melnick, and M. Kaviany, Heterobarrier for converting hot-phonon energy to electric potential, Phys. Rev. B **87**, 075317 (2013).

[9] X. L. Ruan and M. Kaviany, Enhanced laser cooling of rare-earth-ion-doped nanocrystalline powders, Phys. Rev. B **73**, 155422 (2006).

[10] J. Kim and M. Kaviany, Phonon-coupling enhanced absorption of alloyed amorphous silicon for solar photovoltaics, Phys. Rev. B **82**, 134205 (2010).

[11] K. Winer and M. Cardona, Theory of infrared absorption in silicon, Phys. Rev. B **35**, 8189 (1987).

[12] G. Deinzer and D. Strauch, Two-phonon infrared absorption spectra of germanium and silicon calculated from first principles, Phys. Rev. B **69**, 045205 (2004).

[13] J. E. Turney, E. S. Landry, A. J. H. McGaughey, and C. H. Amon, Predicting phonon properties and thermal conductivity from anharmonic lattice dynamics calculations and molecular dynamics simulations, Phys. Rev. B **79**, 064301 (2009).

[14] S. Merabia and K. Termentzidis, Thermal conductance at the interface between crystals using equilibrium and nonequilibrium molecular dynamics, Phys. Rev. B **86**, 094303 (2012).

[15] I. N. Adamenko, K. E. Nemchenko, A. V. Zhukov, M. A. H. Tucker, and A. F. G. Wyatt, Four-phonon scattering in He II, Physica B **284–288**, 31 (2000).

[16] D. Vanderbilt, S. G. Louie, and M. L. Cohen, Calculation of anharmonic phonon couplings in C, Si, and Ge, Phys. Rev. B **33**, 8740 (1986).

[17] D. J. Ecsedy and P. G. Klemens, Thermal resistivity of die ectric crystals due to four-phonon processes and optical modes, Phys. Rev. B **15**, 5957 (1976).

[18] A. A. Maradudin and A. E. Fein, Scattering of neutrons by an anharmonic crystal, Phys. Rev. **128**, 2589 (1962).

[19] G. Deinzer, G. Birner, and D. Strauch, *Ab initio* calculation of the linewidth of various phonon modes in germanium and silicon, Phys. Rev. B **67**, 144304 (2003).

[20] O. Hellman and I. A. Abrikosov, Temperature-dependent effective third-order interatomic force constants from first principles, Phys. Rev. B **88**, 144301 (2013).

[21] J. R. Yates, X. Wang, D. Vanderbilt, and I. Souza, Spectral and Fermi surface properties from Wannier interpolation, Phys. Rev. B **75**, 195121 (2007).

[22] H. J. Monkhorst and J. D. Pack, Special points for Brillouin-zone integrations, Phys. Rev. B **13**, 5188 (1976).

[23] S. Baroni, S. de Gironcoli, A. Dal Corso, and P. Giannozzi, Phonons and related crystal properties from density-functional perturbation theory, Rev. Mod. Phys. **73**, 515 (2001).

[24] X. Gonze and J.-P. Vigneron, Density-functional approach to nonlinear-response coefficients of solids, Phys. Rev. B **39**, 13120 (1989).

[25] P. Giannozzi *et al.*, QUANTUM ESPRESSO: A modular and open-source software project for quantum simulations of materials, J. Phys.: Condens. Matter **21**, 395502 (2009).

[26] M. J. Klein, Principle of detailed balance, Phys. Rev. **97**, 1446 (1955).

[27] V. Spagnolo, M. S. Vitiello, G. Scamarcio, B. S. Williams, S. Kumar, Q. Hu, and J. L. Reno, Hot-phonon generation in THz quantum cascade lasers, J. Phys.: Conf. Ser. **92**, 012018 (2007).

[28] E. T. Swartz and R. O. Pohl, Thermal boundary resistance, Rev. Mod. Phys. **61**, 605 (1989).

[29] S. Shin, M. Kaviany, T. Desai, and R. Bonner, Roles of atomic restructuring in interfacial phonon transport, Phys. Rev. B **82**, 081302 (2010).

[30] A. Dargys and J. Kundrotas, *Handbook on Physical Properties of Ge, Si, GaAs and InP* (Science and Encyclopaedia Publishing Centre, Vilnius, Lithuania, 1994).

[31] Y. Chalopin, K. Esfarjani, A. Henry, S. Volz, and G. Chen, Thermal interface conductance in Si/Ge superlattices by equilibrium molecular dynamics, Phys. Rev. B **85**, 195302 (2012).

[32] H. Hibino and T. Ogino, Trace of interface reconstruction in Ge solid-phase epitaxy on Si(111), Phys. Rev. B **49**, 5765 (1994).

[33] W. M. Haynes (ed.), *CRC Handbook of Chemistry and Physics*, 94th ed. (CRC Press, Boca Raton, FL, 2013).

[34] S. Shin and M. Kaviany, Interflake thermal conductance of edge-passivated graphene, Phys. Rev. B **84**, 235433 (2011).

[35] M. P. Lopez Sancho, J. M. Lopez Sancho, and J. Rubio, Highly convergent schemes for the calculation of bulk and surface Green functions, J. Phys. F **15**, 851 (1985).

[36] J.-S. Wang, X. Ni, and J.-W. Jiang, Molecular dynamics with quantum heat baths: Application to nanoribbons and nanotubes, Phys. Rev. B **80**, 224302 (2009).

[37] W. Zhang, T. S. Fisher, and N. Mingo, The atomistic Green's function method: An efficient simulation approach for nanoscale phonon transport, Numer. Heat Transfer, Part B **51**, 333 (2007).

[38] S. Datta, *Electronic Transport in Mesoscopic Systems* (Cambridge University Press, Cambridge, UK, 1997).

[39] C. Caroli, R. Combescot, P. Nozieres, and D. Saint-James, Direct calculation of the tunneling current, J. Phys. C: Solid State Phys. **4**, 916 (1971).

[40] X. Li and R. Yang, Size-dependent phonon transmission across dissimilar material interfaces, J. Phys.: Condens. Matter **24**, 155302 (2012).

[41] J. Tersoff, Modeling solid-state chemistry: Interatomic potentials for multicomponent systems, Phys. Rev. B **39**, 5566(R) (1989).

[42] Z. T. Tian, K. Esfarjani, and G. Chen, Enhancing phonon transmission across a Si/Ge interface by atomic roughness: First-principles study with the Green's function method, Phys. Rev. B **86**, 235304 (2012).

[43] H. Zhao and J. B. Freund, Lattice-dynamical calculation of phonon scattering at ideal Si-Ge interfaces, J. Appl. Phys. **97**, 024903 (2005).

[44] S. Merabia and K. Termentzidis, Thermal boundary conductance across rough interfaces probed by molecular dynamics, Phys. Rev. B **89**, 054309 (2014).

[45] N. Mingo, Anharmonic phonon flow through molecular-sized junctions, Phys. Rev. B **74**, 125402 (2006).

[46] D. Singh, J. Murthy, and T. Fisher, Effect of phonon dispersion on thermal conduction across Si/Ge interfaces, J. Heat Transfer **133**, 122401 (2011).

[47] X. L. Ruan and M. Kaviany, *Ab initio* photon-electron and electron-vibration coupling calculations related to laser cooling of ion-doped solids, J. Comput. Theor. Nanosci. **5**, 221 (2008).

[48] J. Kim and M. Kaviany, *Ab initio* calculations of *f*-orbital electron-phonon interaction in laser cooling, Phys. Rev. B **79**, 054103 (2009).

[49] J. Noffsinger, E. Kioupakis, C. G. Van de Walle, S. G. Louie, and M. L. Cohen, Phonon-assisted optical absorption in silicon from first principles, Phys. Rev. Lett. **108**, 167402 (2012).

[50] M. Trigo, J. Chen, V. H. Vishwanath, Y. M. Sheu, T. Graber, R. Henning, and D. A. Reis, Imaging nonequilibrium atomic vibrations with x-ray diffuse scattering, Phys. Rev. B **82**, 235205 (2010).

[51] D. Song, F. Wang, G. Dukovic, M. Zheng, E. D. Semke, L. E. Brus, and T. F. Heinz, Direct measurement of the lifetime of optical phonons in single-walled carbon nanotubes, Phys. Rev. Lett. **100**, 225503 (2008).

[52] J. A. Kash, J. C. Tsang, and J. M. Hvam, Subpicosecond time-resolved Raman spectroscopy of LO Phonons in GaAs, Phys. Rev. Lett. **54**, 2151 (1985).

[53] K. T. Tsen, R. P. Joshi, D. K. Ferry, and H. Morkoc, Time-resolved Raman scattering of nonequilibrium LO phonons in GaAs quantum wells, Phys. Rev. B **39**, 1446 (1989).

[54] P. K. Schelling, S. R. Phillpot, and P. Keblinski, Phonon wave-packet dynamics at semiconductor interfaces by molecular-dynamics simulation, Appl. Phys. Lett. **80**, 2484 (2002).

[55] H. Kim and M. Kaviany, Coupled polaron-phonon effects on Seebeck coefficient and lattice conductivity of $B_{13}C_2$ from first principles, Phys. Rev. B **87**, 155133 (2013).

[56] M. Ikezawa and M. Ishigame, Far-infrared absorption due to the two-phonon difference process in Si, J. Phys. Soc. Jpn. **50**, 3734 (1981).

[57] N. A. Roberts and D. G. Walker, A review of thermal rectification observations and models in solid materials, Int. J. Therm. Sci. **50**, 648 (2011).

[58] H. M. van Driel, in *Semiconductors Probed by Ultrafast Laser Spectroscopy*, edited by R. R. Alfano (Academic Press, New York, 1984), Vol. 2, p. 57.

[59] J. Fritsch, P. Pavone, and U. Schröder, *Ab initio* calculation of the phonon dispersion in bulk InP and in the InP(110) surface, Phys. Rev. B **52**, 11326 (1995).

[60] S.-F. Ren, W. Cheng, and P. Y. Yu, Microscopic investigation of phonon modes in SiGe alloy nanocrystals, Phys. Rev. B **69**, 235327 (2004).

[61] M. Maldovan, Sound and heat revolutions in phononics, Nature **503**, 209 (2013).

[62] N. Li, J. Ren, L. Wang, G. Zhang, P. Hänggi, and B. Li, Colloquium: Phononics: Manipulating heat flow with electronic analogs and beyond, Rev. Mod. Phys. **84**, 1045 (2012).